Electronic Supplementary Material (ESI) for Physical Chemistry Chemical Physics.

Supporting information

Na-mobility in P2-$Na_{0.5}Mg_xNi_{0.17-x}Mn_{0.83}O_2$ ($0 \leq x \leq 0.07$) from electrochemical and muon spin relaxation studies

Le Anh Ma*, Rasmus Palm¤, Elisabetta Nocerino¤, Ola Kenji Forslund¤, Nami Matsubara¤, Stephen Cottrell+, Koji Yokoyama+, Akihiro Koda#, Jun Sugiyama$,#,⊥, Yasmine Sassa§, Martin Månsson¤, and Reza Younesi*

* Department of Chemistry-Ångström Laboratory, Uppsala, Sweden

¤ Department of Applied Physics, KTH Royal Institute of Technology, 10691 Stockholm Sweden

+ ISIS Muon Facility, Rutherford Appleton Laboratory, Didcot, Oxfordshire OX11 0QX, UK

High Energy Accelerator Research Organization (KEK), Tokai, Ibaraki 319-1106, Japan

$ Neutron Science and Technology Center, Comprehensive Research Organization for Science and Society (CROSS), Tokai, Ibaraki 319-1106, Japan

⊥ Advanced Science Research Center, Japan Atomic Energy Agency, Tokai, Ibaraki 319-1195, Japan

§ Department of Physics, Chalmers University of Technology, 41296 Gothenburg, Sweden

Table S1. ICP-OES results with standard deviation from average of three replicate measurements.

Sample	**Content**			
P2-$Na_{0.5}Mg_xNi_{0.17-x}Mn_{0.87}O_2$	*Na*	*Mg*	*Ni*	*Mn*
x=0	0.5 ± 0.004	0 ± 0.001	0.17 ± 0.001	0.87 ± 0.009
x=0.02	0.5 ± 0.002	0.02 ± 0.000	0.15 ± 0.001	0.87 ± 0.003
x=0.05	0.5 ± 0.006	0.05 ± 0.000	0.12 ± 0.001	0.87 ± 0.007
x=0.07	0.5 ± 0.007	0.07 ± 0.000	0.10 ± 0.001	0.87 ± 0.004

All samples were pre-characterized using in-house x-ray diffraction (XRD) in order to ensure a successful materials synthesis. Powder X-ray diffraction patterns were recorded on a Rigaku Smartlab (Japan) diffractometer using Cu $K_{\alpha 1}$ radiation (λ = 1.54051 Å) at room temperature. The acquired XRD patterns for all four P2-$Na_{0.5}Mg_xNi_{0.17-x}Mn_{0.87}O_2$ (x = 0, 0.02, 0.05 and 0.07) samples are shown together with simulated pattern based on x = 0 structure in **Fig. S1a** below. With increasing Mg content, the crystallographic unit cell volume clearly displays the expected linear increase due to the larger ionic radius of Mg (see **Fig. S1b**). It was also possible to adequately Rietveld refine the XRD data using the Fullprof software suite[1] (see **Fig. S1c**) and

extract the atomic positions, fractional site occupancies, and so on. Such data is presented and used in the main article (**Fig.1** and **Fig. 5**). Further, it is clear that the sample is of high quality and only minor impurity peaks are present (see inset of **Fig. S1c**). It is possible to identify such peaks as unreacted synthesis starting materials, e.g. NiO (blue arrow of the inset in **Fig. S1c**) and MnO (orange arrow of the inset in **Fig. S1c**), which both have a hexagonal space group. We can also estimate that such impurity phases constitute less than 5% of the sample volume.

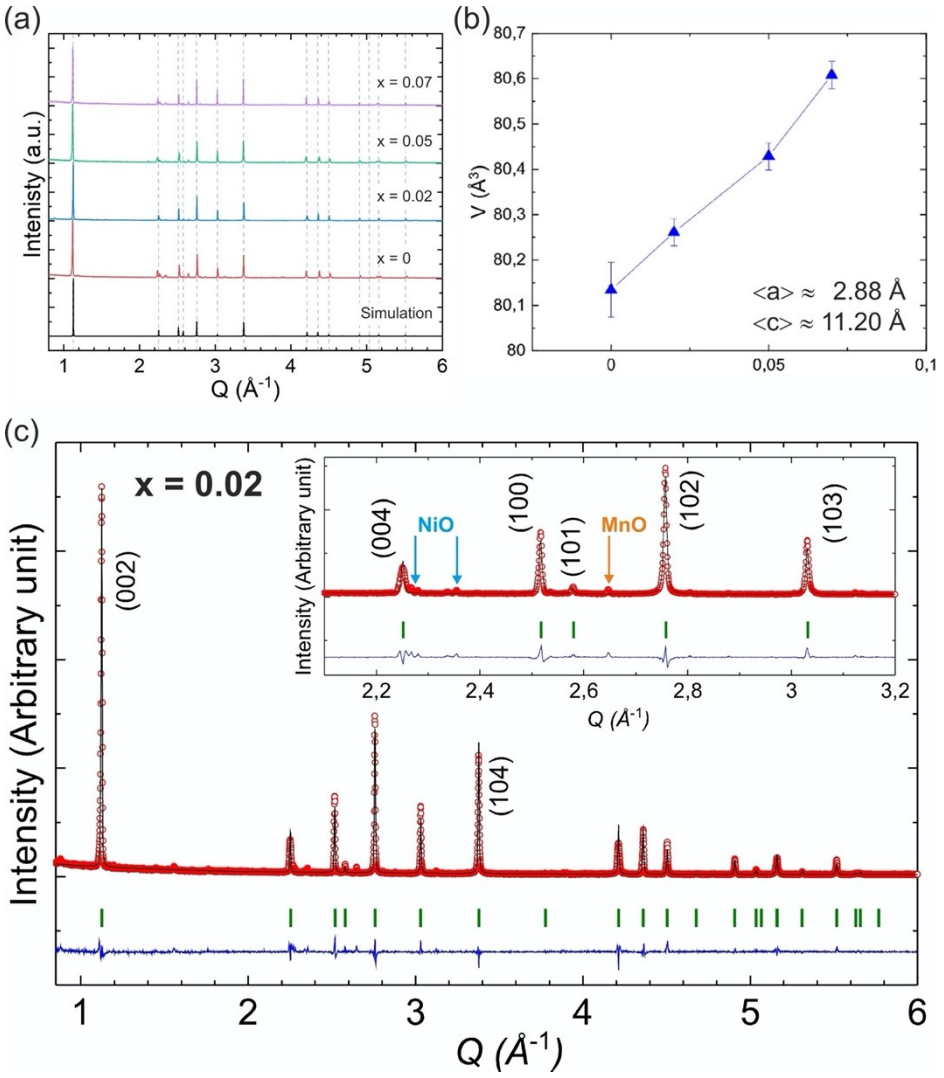

Fig. S1 (a) XRD pattern of P2-$Na_{0.5}Mg_xNi_{0.17-x}Mn_{0.87}O_2$ (x = 0, 0.02, 0.05 and 0.07) samples together with a simulated pattern based on x = 0 structure. (b) Cell volume for different Mg-content (x) along with the average lattice parameters <a> and <c>. (c) Rietveld refinement of the XRD data for the x = 0.02 sample. The inset show minor impurity phases (≤ 5%) most likely corresponding to nickel and manganese oxide compounds, which could partially come from unreacted synthesis starting materials (NiO and MnO). The starting materials are marked by blue (NiO, hexagonal) and orange (MnO, hexagonal) arrows, respectively and represent possible compounds.

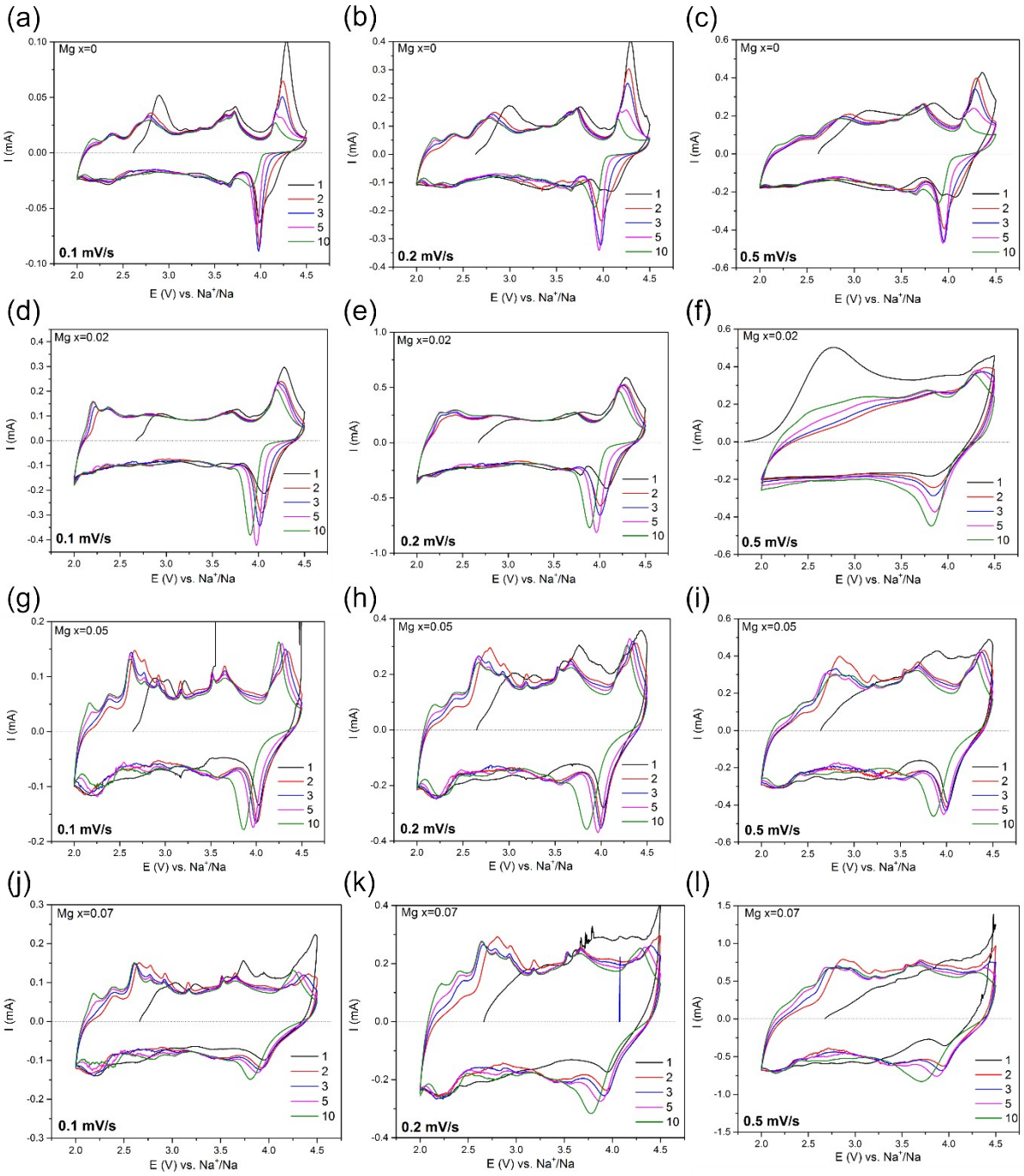

Fig. S2 Cyclic voltammetry (CV) measurements for all P2-$Na_{0.5}Mg_xNi_{0.17-x}Mn_{0.87}O_2$ (x = 0, 0.02, 0.05 and 0.07) samples at three different scan rates (0.1 mV/s, 0.2 mV/s and 0.5 mV/s) in a voltage range of 2.0 – 4.5 V vs. Na^+/Na. The scan starts at OCV to 4.5 V, and then scans back to 2.0 V, completing one cycle. (a)-(c) CV curves of $Na_{0.5}Ni_{0.17}Mn_{0.87}O_2$ at scan rates of 0.1 mV/s, 0.2 mV/s and 0.5 mV/s. (d)-(f) CV curves of $Na_{0.5}Mg_{0.02}Ni_{0.15}Mn_{0.87}O_2$ at scan rates of 0.1 mV/s, 0.2 mV/s and 0.5 mV/s. (g)-(i) CV curves of $Na_{0.5}Mg_{0.05}Ni_{0.12}Mn_{0.87}O_2$ at scan rates of 0.1 mV/s, 0.2 mV/s and 0.5 mV/s. The curve scanned at 0.1 mV/s has noise signals at higher voltage ranges in the first scan due to cable interruption which will be disregarded for further analyses. (j)-(l) CV curves of $Na_{0.5}Mg_{0.07}Ni_{0.10}Mn_{0.87}O_2$ at scan rates of 0.1 mV/s, 0.2 mV/s and 0.5 mV/s. The curve scanned at 0.2 mV/s has noise signal in the first scan due to minor cable interruption which will be disregarded for further analyses.

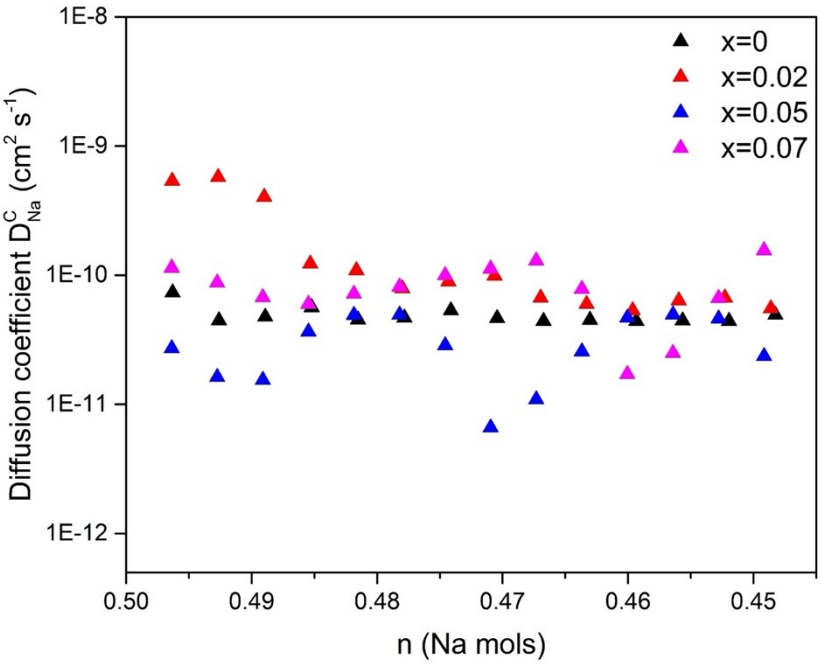

Fig. S3 Chemical diffusion coefficient as a function of the molar Na-concentration in the electrode determined from GITT measurements for P2-$Na_{0.5}Mg_xNi_{0.17-x}Mn_{0.87}O_2$ (x = 0, 0.02, 0.05 and 0.07).

Chemical diffusion coefficient of Na-ions (D_{Na}^C) is calculated by the following equation[2]:

$$D_{Na}^{C} = \frac{4}{\pi}\left(\frac{i\,V_m}{z_A F S}\right)^2 \left(\frac{\frac{dE}{d\delta}}{\frac{dE}{d\sqrt{t}}}\right)^2 \qquad \text{(Eq. S1)}$$

i: pulse current [A], 2 μA/mg (based on active material)

V_m: molar volume [cm^3/mol], obtained from lattice parameters

z_A: charge number, 1 for Na^+/Na

F: Faraday constant [A·s/mol], 96486 As/mol

S: Electrode surface area [cm^2], here: S = 5.31 cm^2

d*E*/dδ: Steady state voltage changes after each titration step δ [V/n], where n is the molar Na-concentration in the electrode)

d*E*/d$\sqrt{t}$: Voltage changes during a current pulse in relation to $\sqrt{t}$

Note that this equation is based on a one-dimensional diffusion in a solid solution electrode, neglecting several processes, such as double-layer charging, ohmic potential drop (iR-drop), phase transitions and charge-transfer kinetics.[2–4] However, for this study it was used to highlight the trend in chemical diffusion coefficients based on the Mg-substitution.

Muon Spin Rotation and Relaxation (μ^+SR) Experimental Details

The μ^+SR experiments were performed at both ISIS pulsed muon source (UK) using the EMU[5] instrument as well as J-PARC MLF pulsed muon source (Japan) using the S1 beamline[6]. For both experiments approximately 1.5 grams of powder sample was pressed into a ∅ = 23 mm pellet using a special pressing tool (see **Fig. S4a)**. The thickness of the pellet $t \approx 1.5$ mm, which together with the density of the compound ensures that all implanted mouns are effectively stopped only inside the sample. The pellet is placed (see **Fig. S4b**) inside a sample cell made of titanium (grade 5, non-magnetic), which is hermetically sealed using a gold O-ring (see **Fig. S4c**) and a very thin (25 μm) titanium window using titanium bolts (see **Fig. S4d)**. The sealed sample cell is then finally mounted onto the closed-cycle cryostat (CCR) cold finger together with a mask of ultra-pure silver. The mask has a circular whole matching both sample size along with muon beam spot size and center. The mask ensures that any muons hitting outside the actual sample location will only generate a flat and temperature independent background signal.

The μ^+SR time spectrum was recorded as a function of temperature (always on heating) in the temperature range $T \approx 50 - 450$ K. At each temperature, a series of measurements were performed using different external field protocols. First, a zero-field (ZF) time spectrum is acquired, followed by two to three spectra under longitudinal field (LF = 5, 20 and 40 G). Here, LF refers to an externally applied field that is parallel to the initial muon spin polarization.[7] The reason for acquiring multiple ZF and LF spectra at each temperature is to obtain a robust and high-quality fit of multiple fitting parameters (see further details below). Finally, the transverse field (TF) μ^+SR spectrum at each temperature was used to calibrate the background level as well as an extra security check that sample holder and/or muon beam got misaligned during the temperature scan. Here transverse means that the field direction is perpendicular to the initial muon spin.[7]

It should also be noted that the room-temperature measurements were conducted in total 3 times: (1) Initially directly after sample mounting. (2) Upon heating within the temperature dependent series of measurements. (3) At the end of the measurement after cooling back down to room-temperature in order to ensure that sample did not change/decompose. For all samples no changes in the signal were detected in any of the data sets (= samples are stable).

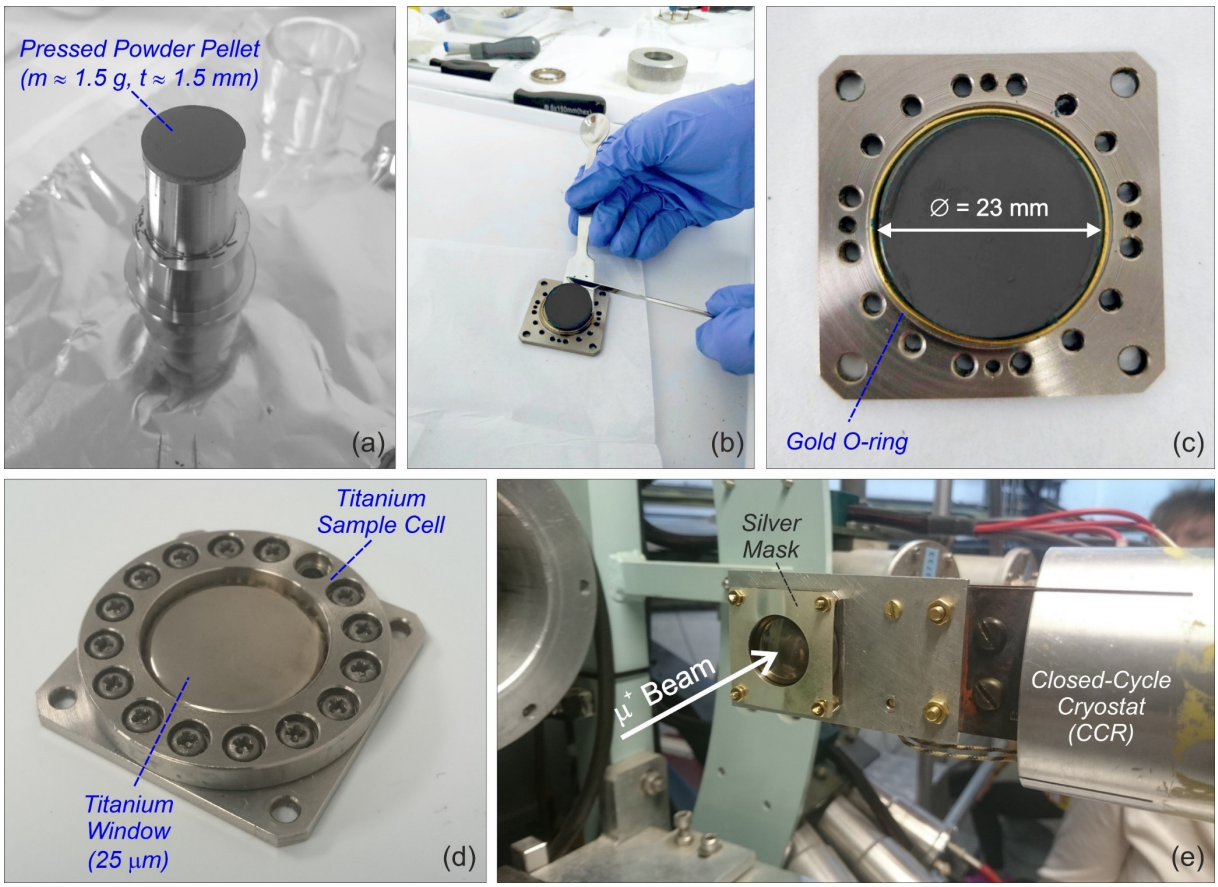

Fig. S4 Sample preparation and mounting for the μ^+SR experiments: **(a)** Powder sample ($m \approx$ 1.5 gram) is pressed into a pellet (diameter $\varnothing \approx$ 23 mm and thickness $t \approx$ 1.5 mm) using a dedicated pressing tool. **(b)** Sample pellet is put inside the **(c)** titanium (grade 5, non-magnetic) sample cell that is hermetically sealed using a gold o-ring. **(d)** Sealed titanium sample cell with the 25 μm thin titanium foil/window covering the sample. **(e)** Ti-cell is then mounted onto the closed-cycle cryostat (CCR) and covered by a mask made of ultra-pure silver. The mask has a circular hole matching the center and size of the muon beam. Photos are from the EMU instrument of ISIS (UK), but a very similar setup is used at the S1 beamline of J-PARC MLF (Japan).

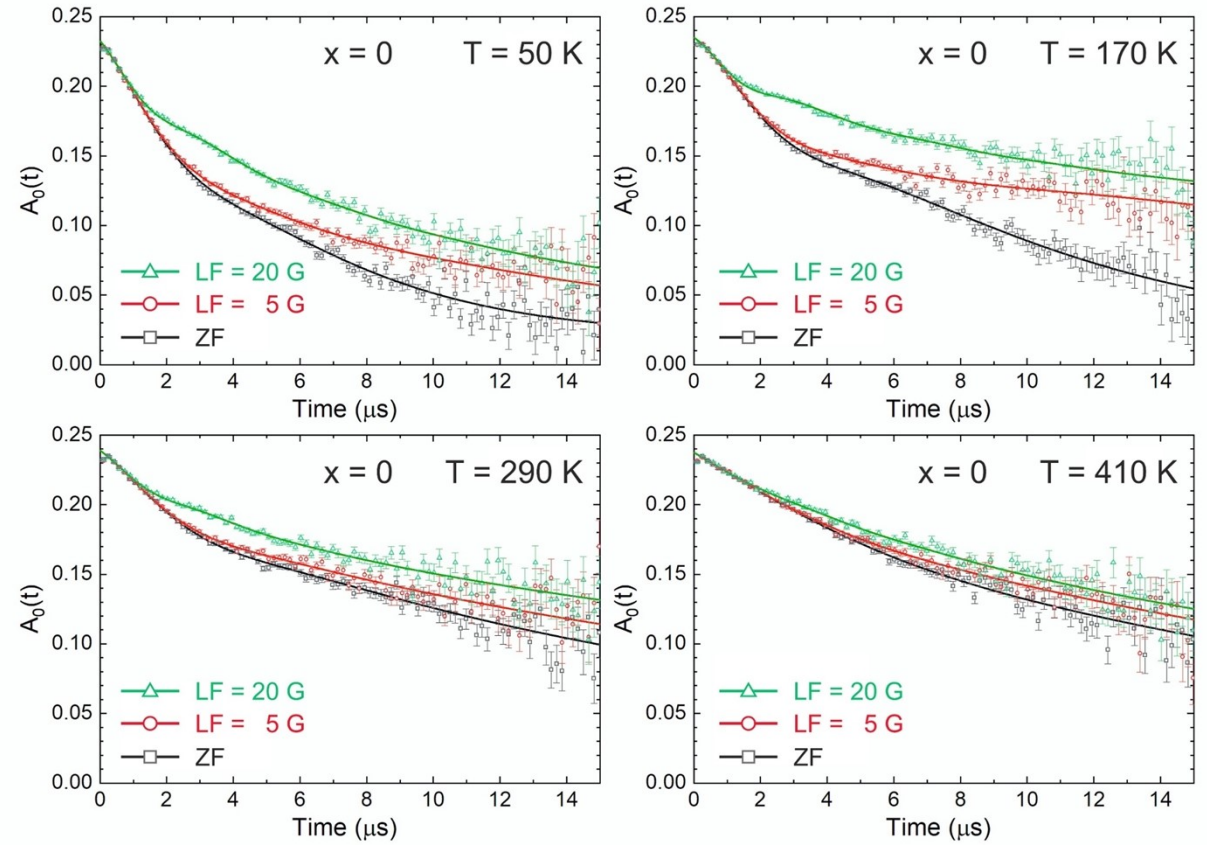

Fig.S5 μ^+SR raw-data (zero-field, ZF, as well as longitudinal-field, LF, protocols) for the *x* = 0 sample is shown as open symbols together with the corresponding global fits (solid lines) using **Eq. S2** for selected temperatures. For all temperatures, the fitting procedure generates a good fit to the data in the entire time-range.

μ^+SR Data Analysis

The ZF and two or three LF (= 5, 20 and/or 40 G, respectively) μ^+SR time spectra (shown in **Fig. S5**) for each temperature were fitted globally in order to obtain a robust determination of all the fit parameters. The fit function used was a combination of two exponentially relaxing Gaussian Kubo-Toyabe (KT) functions[8] (G_{KT}) and a background (BG) signal:

$$A_0P(t) = A_{KT1} \cdot G_{KT1}(\Delta_1,\nu_1,t) \cdot e^{-\lambda_1 t} + A_{KT2} \cdot G_{KT2}(\Delta_2,t) \cdot e^{-\lambda_2 t} + A_{BG} \qquad \text{(Eq. S2)}$$

Here KT1 is a dynamic gaussian KT function that constitutes the majority signal, which also yield the dynamic properties of the sodium ions. This function has two fitting parameters: Δ_1 that is the static field distribution width (at the muon site) and ν_2 that is the field fluctuation rate. In the paramagnetic state of P2-$Na_{0.5}Mg_xNi_{0.17-x}Mn_{0.87}O_2$ the main dynamic contribution, i.e. ν, comes from the nuclear magnetic moment of sodium. For such case, the field fluctuation rate directly translates into an Na-ion hopping rate (in μs^{-1}).[9,10] The second fit function component (KT2) is static Gaussian KT function that only contains a static Δ_2 (i.e. ν_2 is fixed to zero). It has

a very low asymmetry ($A_{KT2} \approx 0.01$), which equals less than 5% of the sample volume. Such minor phase is in perfect agreement with the XRD results and can be readily assigned to the tiny NiO/MnO impurity phase (see **Fig. S1** above), which naturally cannot display any Na-ion diffusion. Both the KT1 and KT2 functions are multiplied by an exponentially relaxing function, which is there to model the highly dynamic electronic spins of the paramagnetic (PM) Ni atoms. Finally, another minor and non-relaxing component (A_{BG}) is added that corresponds to the few muons that stop outside the sample, i.e. in the silver mask (see also **Fig. S4e**). As seen from **Fig.. S5**, **Eq. S1** very nicely fit all the ZF and LF- time spectra within the entire temperature range. It should be however noted that at higher temperatures (starting just below $T \approx 400$ K), even though the fit to the data looks basically fine, the extracted fit parameters Δ and ν are not fully reliable. This is due to the limited accessible timeframe of μ^+SR (average muon lifetime is only 2.2 μsec)[7] and when the vital features of the KT function appears beyond 15-20 μsec, output from fitting procedure becomes ambiguous. In order to present only robust, systematic and reliable results, we have therefore chosen to omit the higher temperatures (fit results) from the analysis of activation energy and self-diffusion coefficient. However, for full transparency we still show the raw-data and fits in **Fig. S5**.

The temperature dependence of the field fluctuation rate (ν), that in this case translates into the Na-ion hopping rate, is shown in **Fig. 5a-d** (main article). Here a constant background (mainly coming from electronic fluctuations) of approximately 0.05 μs^{-1} has been subtracted from all samples in order to yield an Arrhenius fit of the Na-ion dynamics with zero base level.

Finally, the TF-μ^+SR spectrum at each temperature (see **Fig. S6**) was used to calibrate the background level as well as serves as an extra security check in case the sample holder and/or muon beam got misaligned during the temperature scan (which was found not to have happened during the entire experiment). The TF-spectra were fitted using a simple exponentially relaxing oscillating cosine function:

$$A_0 P_{TF}(t) = A_{TF} \cdot \cos(\omega t + \phi) \cdot e^{-\lambda_{TF} t} \quad \text{(Eq. S3)}$$

Here A_{TF} is the asymmetry (intensity) of the signal and ω the angular frequency of the oscillation (note that $\omega = 2\pi \cdot TF \cdot \gamma_\mu$ where TF = 20 G, i.e. the applied field and γ_μ = 135.5 MHz/T is the gyromagnetic ratio of the muon)[7]. Further, ϕ is the phase of the oscillation and λ_{TF} the relaxation rate.

The entire μ⁺SR fitting procedure (ZF, LF and TF) was conducted using the **musrfit** open software suite.[11]

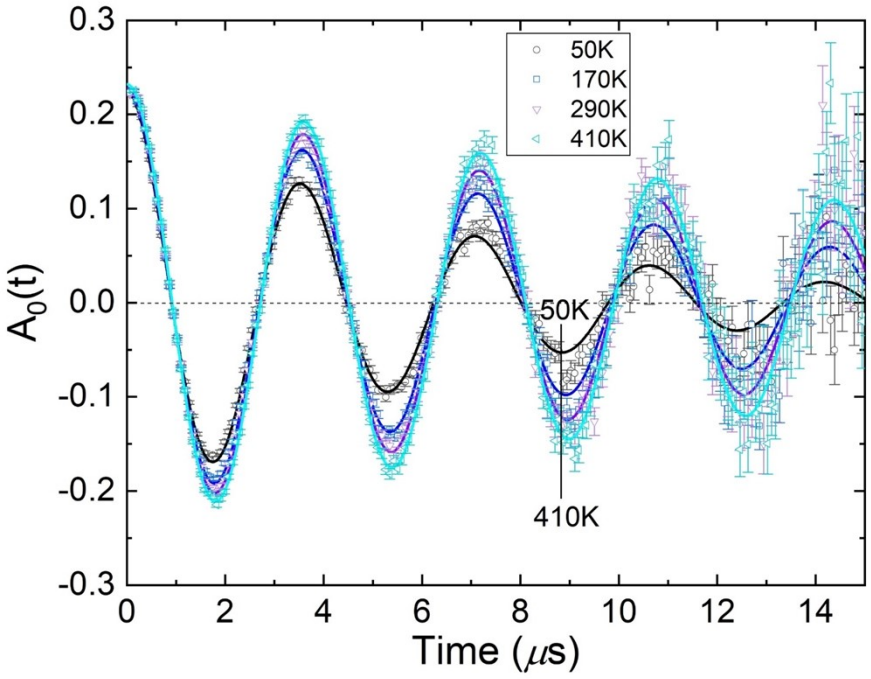

Fig. S6 Weak transverse field (wTF = 20 G) μ⁺SR time spectra as a function of temperature for the parent compound (x = 0). Solid lines are fits to a simple exponentially relaxing oscillating cosine function, as specified by **Eq. S3**.

Tab. S2 Na^+-ion hopping rates (ν) calculated for all sample compositions and selected temperatures using the Arrhenius parameters extracted from the fits of the μ⁺SR data (see **Figure 5a-d** and **Tab. 1** of the main article).

Temperature [°C]	ν [μs^{-1}] x = 0	ν [μs^{-1}] x = 0.02	ν [μs^{-1}] x = 0.05	ν [μs^{-1}] x = 0.07
-50	0.0906	0.1778	0.0212	0.0202
-25	0.1546	0.2796	0.0432	0.0412
0	0.2391	0.4046	0.0771	0.0736
25 (Room-T)	0.3438	0.5503	0.1249	0.1193
50	0.4673	0.7137	0.1877	0.1796
100	0.7633	1.0813	0.3600	0.3450

Tab. S3 Na^+-ion self-diffusion coefficients ($^{\mu}D_{Na^+}{}^{J}$) calculated for all sample compositions and selected temperatures using the hopping rates (ν) from **Tab. S2** inserted into **Eq. 2** of the main article (resulting data is also summarized in **Fig. 7** of the main article).

Temperature [°C]	$^{\mu}D_{Na}{}^{J}$ [$cm^2 \cdot s^{-1}$] × 10^{-10} x = 0	$^{\mu}D_{Na}{}^{J}$ [$cm^2 \cdot s^{-1}$] × 10^{-10} x = 0.02	$^{\mu}D_{Na}{}^{J}$ [$cm^2 \cdot s^{-1}$] × 10^{-10} x = 0.05	$^{\mu}D_{Na}{}^{J}$ [$cm^2 \cdot s^{-1}$] × 10^{-10} x = 0.07
-50	0.1245	0.2464	0.0293	0.0280
-25	0.2125	0.3873	0.0595	0.0570
0	0.3287	0.5605	0.1062	0.1019
25 (Room-*T*)	0.4726	0.7623	0.1720	0.1652
50	0.6424	0.9887	0.2586	0.2486
100	1.0491	1.4980	0.4961	0.4776

References

1 J. Rodríguez-Carvajal, Recent advances in magnetic structure determination by neutron powder diffraction, *Phys. B Phys. Condens. Matter*, 1993, **192**, 55–69.

2 Y. Zhu and C. Wang, Galvanostatic intermittent titration technique for phase-transformation electrodes, *J. Phys. Chem. C*, 2010, **114**, 2830–2841.

3 A. Nickol, T. Schied, C. Heubner, M. Schneider, A. Michaelis, M. Bobeth and G. Cuniberti, GITT Analysis of Lithium Insertion Cathodes for Determining the Lithium Diffusion Coefficient at Low Temperature: Challenges and Pitfalls, *J. Electrochem. Soc.*, 2020, **167**, 090546.

4 E. Deiss, Spurious chemical diffusion coefficients of Li+ in electrode materials evaluated with GITT, *Electrochim. Acta*, 2005, **50**, 2927–2932.

5 S. R. Giblin, S. P. Cottrell, P. J. C. King, S. Tomlinson, S. J. S. Jago, L. J. Randall, M. J. Roberts, J. Norris, S. Howarth, Q. B. Mutamba, N. J. Rhodes and F. A. Akeroyd, Optimising a muon spectrometer for measurements at the ISIS pulsed muon source, *Nucl. Instruments Methods Phys. Res. Sect. A Accel. Spectrometers, Detect. Assoc. Equip.*, 2014, **751**, 70–78.

6 Y. Miyake, K. Shimomura, N. Kawamura, A. Koda, P. Strasser, K. M. Kojima, H. Fujimori, S. Makimura, Y. Ikedo, Y. Kobayashi, J. Nakamura, Y. Oishi, S. Takeshita, T. Adachi, A. D. Pant, H. Okabe, S. Matoba, M. Tampo, M. Hiraishi, K. Hamada, S. Doiuchi, W. Higemoto, T. U. Ito and R. Kadono, J-PARC Muon Facility, MUSE, *JPS Conf. Proc.*, 2018, **21**, 011054.

7 A. Yaouanc and P. Dalmas De Reotier, *Muon Spin Rotation, Relaxation, and Resonance Applications to Condensed Matter*, Oxford University Press, Oxford, 2011.

8 R. Kubo and T. Toyabe, *Magnetic Resonance and Relaxation*, North-Holland, Amsterdam, 1967.

9 J. Sugiyama, K. Mukai, Y. Ikedo, H. Nozaki, M. Månsson and I. Watanabe, Li diffusion in lixCoO2 probed by Muon-Spin spectroscopy, *Phys. Rev. Lett.*, 2009, **103**, 147601.

10 M. Månsson and J. Sugiyama, Muon-spin relaxation study on Li- and Na-diffusion in solids, *Phys. Scr.*, 2013, **88**, 068509.

11 A. Suter and B. M. Wojek, Musrfit: A Free Platform-Independent Framework for μsR Data Analysis, *Phys. Procedia*, 2012, **30**, 69–73.